WILEY-VCH

DOI: 10.1002/ ((please add manuscript number))

Article type: Communication

A non-volatile chalcogenide switchable hyperbolic metamaterial

*Harish N. S. Krishnamoorthy, Behrad Gholipour, Nikolay I. Zheludev, and Cesare Soci**

Dr. Harish N. S. Krishnamoorthy, Prof. Nikolay I. Zheludev, Prof. Cesare Soci

Centre for Disruptive Photonic Technologies, TPI, SPMS, Nanyang Technological University, Singapore 637371
Email: csoci@ntu.edu.sg

Dr. Behrad Gholipour, Prof. Nikolay I. Zheludev

Optoelectronics Research Centre & Centre for Photonic Metamaterials, University of Southampton, SO17 1BJ, Southampton, UK

Keywords: phase change, non-volatile, chalcogenide, hyperbolic, metamaterial

Abstract: **Phase change materials have enabled the realization of dynamic nanophotonic devices with various functionalities. Reconfigurable hyperbolic metamaterials integrated with such elements have been demonstrated in the past but the volatile nature of their optical properties has been a limitation, particularly for applications that require the device to be preserved in a specified state. Here, we report the first proof-of-concept demonstration of a non-volatile, switchable hyperbolic metamaterial based on a chalcogenide glass. By using the $Ge_2Sb_2Te_5$ (GST) alloy as one of the components of a multilayered nanocomposite structure and exploiting its phase change property, we demonstrate a hyperbolic metamaterial in which the type-I hyperbolic dispersion ($\varepsilon_\perp < 0$, $\varepsilon_\parallel > 0$) and negative refraction can be switched from the near-infrared to the visible region. This opens up new opportunities for reconfigurable device applications, such as imaging, optical data storage and sensing.**

Metal-dielectric nanocomposite structures have attracted considerable interest over the last decade owing to their ability to support electron charge oscillations, known as surface plasmon polaritons. An example of such systems are hyperbolic metamaterials (HMMs), strongly anisotropic systems where the coupling between multiple surface plasmon polariton modes gives rise to a characteristic hyperbolic optical isofrequency surface, which supports electromagnetic states with large wave vectors.[1] These peculiar properties lead to unusual effects such as negative refraction [2–4] as well as nominally infinite photonic density of states,[5] and have been exploited for a variety of applications such as optical imaging beyond the diffraction limit,[6,7] enhancing spontaneous emission rates of quantum emitters,[8–10] efficient heat transfer,[11,12] epsilon-near-zero perfect absorption[13], nanoscale indefinite cavities,[14,15] and optical sensing.[16] Unlike resonant systems such as microcavities and nanoscale resonator arrays, hyperbolic metamaterials exhibit their extraordinary electromagnetic properties over a wide spectral range, thereby making them useful for applications that require broadband response.

The principal characteristics of an HMM such as the nature of the hyperbolic dispersion and its onset frequency are determined by the constituent metal and dielectric materials as well as their relative fill-fraction, and usually cannot be changed once the HMM is fabricated. The ability to dynamically tune the topology of the optical isofrequency surface is significant as it can lead to the realization of tunable hyperlenses, reconfigurable light emitting devices, and sensors. Moreover, future optical networks will require a new generation of adaptable integrated nanophotonic devices with functions such as optical switching and mode (de)multiplexing. Consequently, phase change materials are gathering growing interest to realise reconfigurable photonic devices. In this pursuit, phase change materials such as vanadium dioxide and chalcogenide glasses have emerged as

unique platforms for realising optically reconfigurable metamaterials,[17] metasurfaces,[18–22] and volatile tunable HMMs.[23–27]

In particular, chalcogenide compounds (binary and ternary sulphides, selenides and tellurides) are an exceptionally adaptable phase change material base, thanks to their compositionally-controlled high-index and low optical losses throughout a broad spectral range, from the visible to the far-infrared. These, combined with their non-volatile, reversible switching properties, which are easily triggered by thermal, electrical or optical means, have made them the materials of choice for a range of photonic devices with applications in mid-infrared sensing, integrated optics and ultrahigh-bandwidth signal processing.[28–31] Notably, phase-change properties of chalcogenides – reversible transitions between amorphous and crystalline states with starkly different optical (refractive index) and electronic (conductivity) characteristics, have been exploited for decades in optical data storage and more recently in electronic phase-change random access memories.[32,33]

Here we utilise the chalcogenide alloy $Ge_2Sb_2Te_5$ (GST) as the non-volatile switchable constituent of a multilayer HMM. By exploiting the reversible amorphous to crystalline phase transition of GST, we demonstrate the first chalcogenide-based non-volatile reconfigurable HMM. As a proof-of-concept, we show that the sign of refraction of an incident TM polarized light beam in the near-infrared (NIR) spectral region can be switched from negative to positive, as shown schematically in **Figure 1**. In contrast to previous demonstrations of tunable HMMs based on vanadium dioxide,[23] graphene,[24,25] liquid crystals[26] and Kerr nonlinearity,[27] our approach based on chalcogenide glass as the switchable medium produces HMMs that are inherently non-volatile. In other words, the HMM can be kept in a chosen state without the need for external factors such as heat or electric field.

One of the most common approaches employed to realize an HMM is to fabricate a multilayer stack composed of alternate metal and dielectric layers of subwavelength thicknesses as shown schematically in Figure 1. In the effective medium limit, the dielectric permittivity tensor of such a layered nano-composite takes the form, $\vec{\vec{\varepsilon}}(\vec{r}) = diag(\varepsilon_{xx}, \varepsilon_{yy}, \varepsilon_{zz})$, where $\varepsilon_{xx} = \varepsilon_{yy} = \varepsilon_{\parallel}$ and $\varepsilon_{zz} = \varepsilon_{\perp}$ are the effective dielectric constants of the structure in the direction parallel and perpendicular to the plane of the layers, respectively. Depending on the sign of the effective dielectric constants, the dispersion relation for light interacting with the HMM can be elliptical $[real(\varepsilon_{\perp}, \varepsilon_{\parallel}) > 0]$, hyperbolic type-I $[real(\varepsilon_{\perp} < 0), real\ (\varepsilon_{\parallel} > 0)]$ or hyperbolic type-II $[real(\varepsilon_{\perp} > 0), real\ (\varepsilon_{\parallel} < 0)]$.

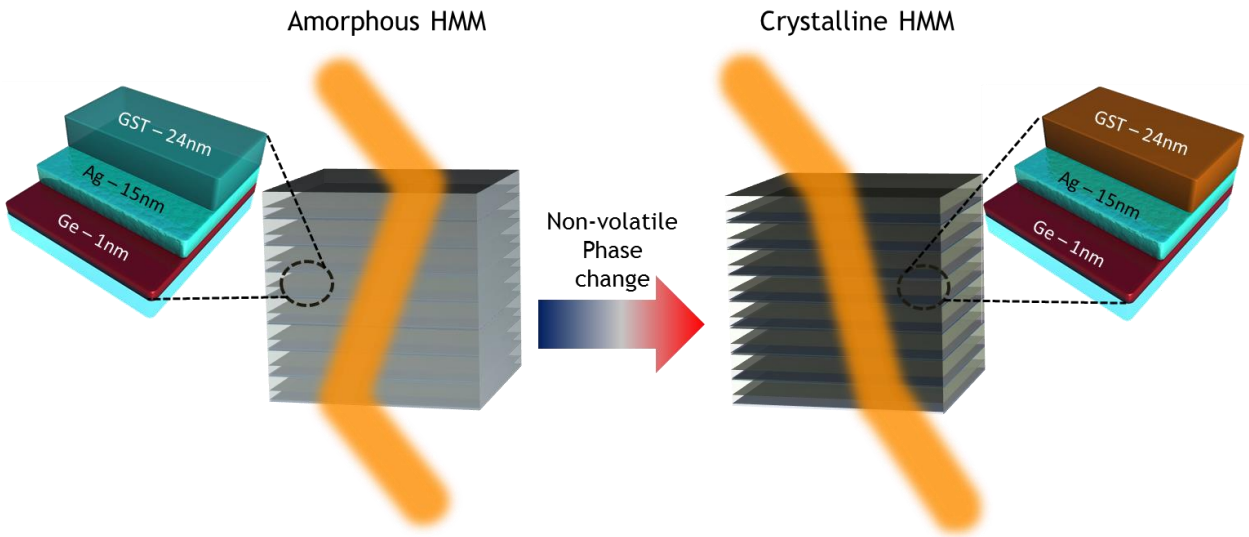

Figure 1. Schematic of the chalcogenide-based hyperbolic metamaterial in the as-deposited configuration with the GST layers in the amorphous phase and after crystallization of GST layers by thermal annealing. In the former configuration, the HMM shows negative refraction for incident near-IR light while in the latter, the sign of refraction is reversed by thermal annealing of the metamaterial. The HMM is comprised of seven periods of Ge, Ag and GST layers.

In our experiments, the HMM comprises of 7 periods of alternating layers of silver (Ag) and GST of thicknesses 15 nm and 24 nm, respectively, as shown schematically in Figure 1. An ultrathin layer (~ 1 nm thick) of germanium (Ge) is used as a wetting layer in order to ensure good

quality silver films.[34] The HMM was deposited on optically flat quartz substrates by RF sputtering (Kurt J. Lesker Nano 38). A base pressure of 5 x 10^{-5} mbar is achieved prior to deposition and high-purity argon is used as the sputtering gas. The substrate is held within 10 K of room temperature on a rotating plate 150 mm from the target to produce low-stress as-deposited amorphous films. The layer thicknesses were ascertained by means of a quartz crystal thickness monitor whose parameters for Ag, GST and Ge were calibrated based on stylus profilometer measurements on the respective single layers deposited separately.

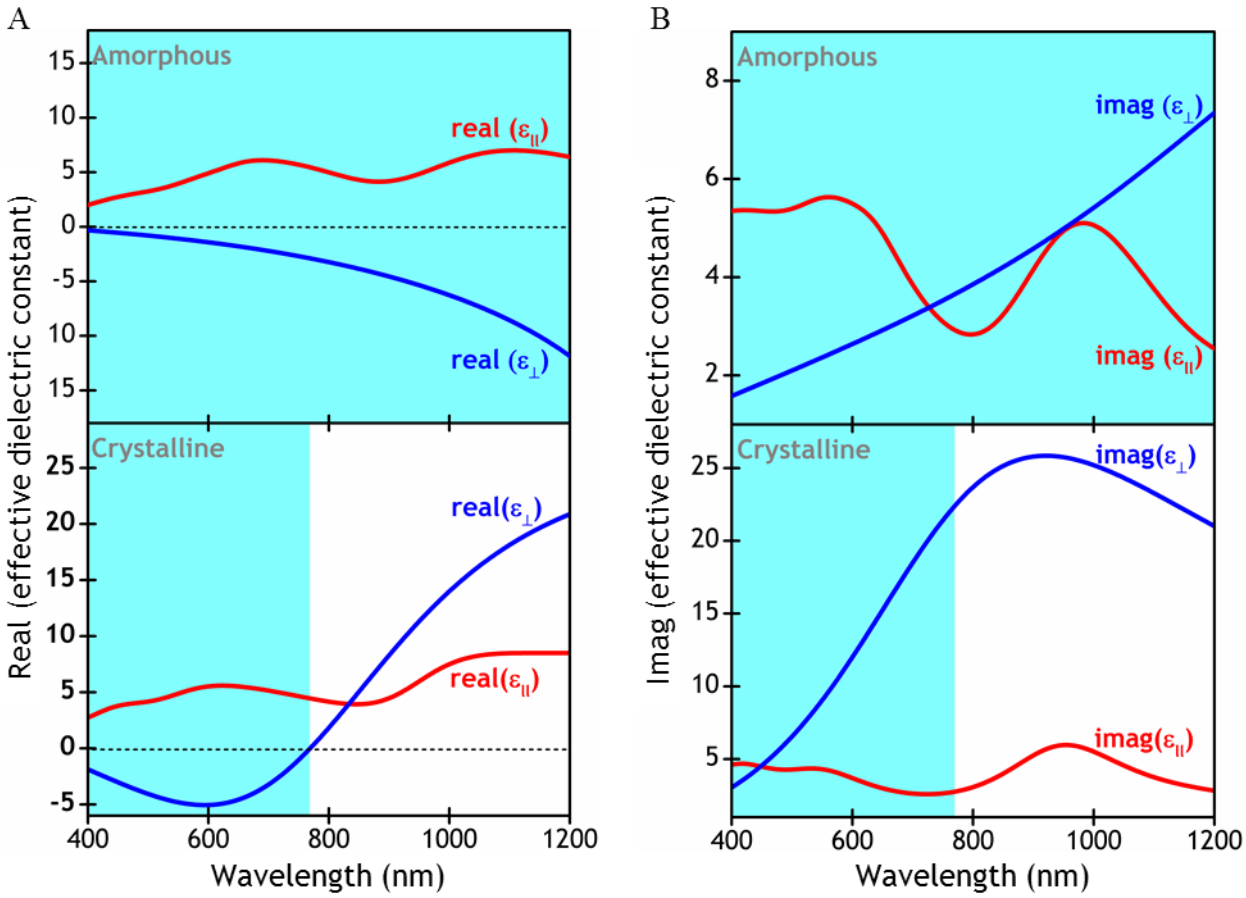

Figure 2. (A) Real and (B) imaginary parts of the effective dielectric constants $\varepsilon_{\parallel}$ and $\varepsilon_{\perp}$ of the HMM extracted from ellipsometry, with GST layers in the amorphous (top panel) and crystalline (bottom panel) phases. The shaded part indicates the region of hyperbolic dispersion.

Optical characterization of the HMM was performed by carrying out spectroscopic ellipsometric measurements using a J. A. Woollam M2000 ellipsometer, over a broad spectral range of 250 – 1500 nm, at multiple angles. The experimental data were analysed using a uniaxial anisotropic model[4,35] to extract the effective in-plane ($\varepsilon_{\parallel}$) and out-of-plane ($\varepsilon_{\perp}$) dielectric constants of the HMM. The advantage of employing such a model is that it treats the HMM as an optically anisotropic 'blackbox' and enables understanding of the HMM's optical response without the knowledge of the dielectric constants of the individual layers composing the HMM. The top panels of **Figures 2A** and **2B** show the real and imaginary parts of effective dielectric constants of our HMM in the as-deposited configuration, with the GST layers in the amorphous phase. The structure exhibits type-I hyperbolic dispersion with $real(\varepsilon_{\perp}) < 0$, $real(\varepsilon_{\parallel}) > 0$ in the visible and NIR spectral regions. Subsequently, the HMM is annealed at 300ºC in an argon atmosphere for 5 minutes. This temperature is chosen so as to be above the GST glass-transition point T_g but below its melting point T_m (around 110 ºC and 630 ºC, respectively),[36] to convert the GST phase from amorphous to crystalline. Real and imaginary parts of the effective dielectric constants of the annealed nanocomposite extracted from ellipsometry measurements are shown in the bottom panels of Figures 2A and 2B, respectively; crystallization of the GST layers changes the dispersion of the effective dielectric constants in the NIR region with both $\varepsilon_{\perp}$ and $\varepsilon_{\parallel}$ being positive, yielding an ellipsoidal optical isofrequency surface. The HMM, however still retains type-I hyperbolic dispersion in the visible region. The phase transition within the GST layers also affects the imaginary part of the dielectric constant significantly – the HMM has larger overall losses with the GST layers in the crystalline phase (bottom panel of Figure 2B) which is consistent with the optical response of a typical crystallized GST layer.[18]

The HMMs in both phases were characterized further by carrying out polarized reflection measurements as a function of incidence angle. We compared the results of these measurements

with the reflectivity spectra calculated based on a uniaxially anisotropic model, using the effective dielectric constants in Figure 2. **Figures 3A** and **3B** show the good agreement between the measured and calculated reflection spectra for TM polarization, for both as-deposited and annealed HMM samples. Similar measurements with TE polarized light also showed good agreement between the experimental and calculated spectra (see Supporting Information). This confirms that the techniques as well as the anisotropic ellipsometry model used to retrieve the effective dielectric constants of the HMMs in the two phases are reliable and provide a proper description of the optical response.

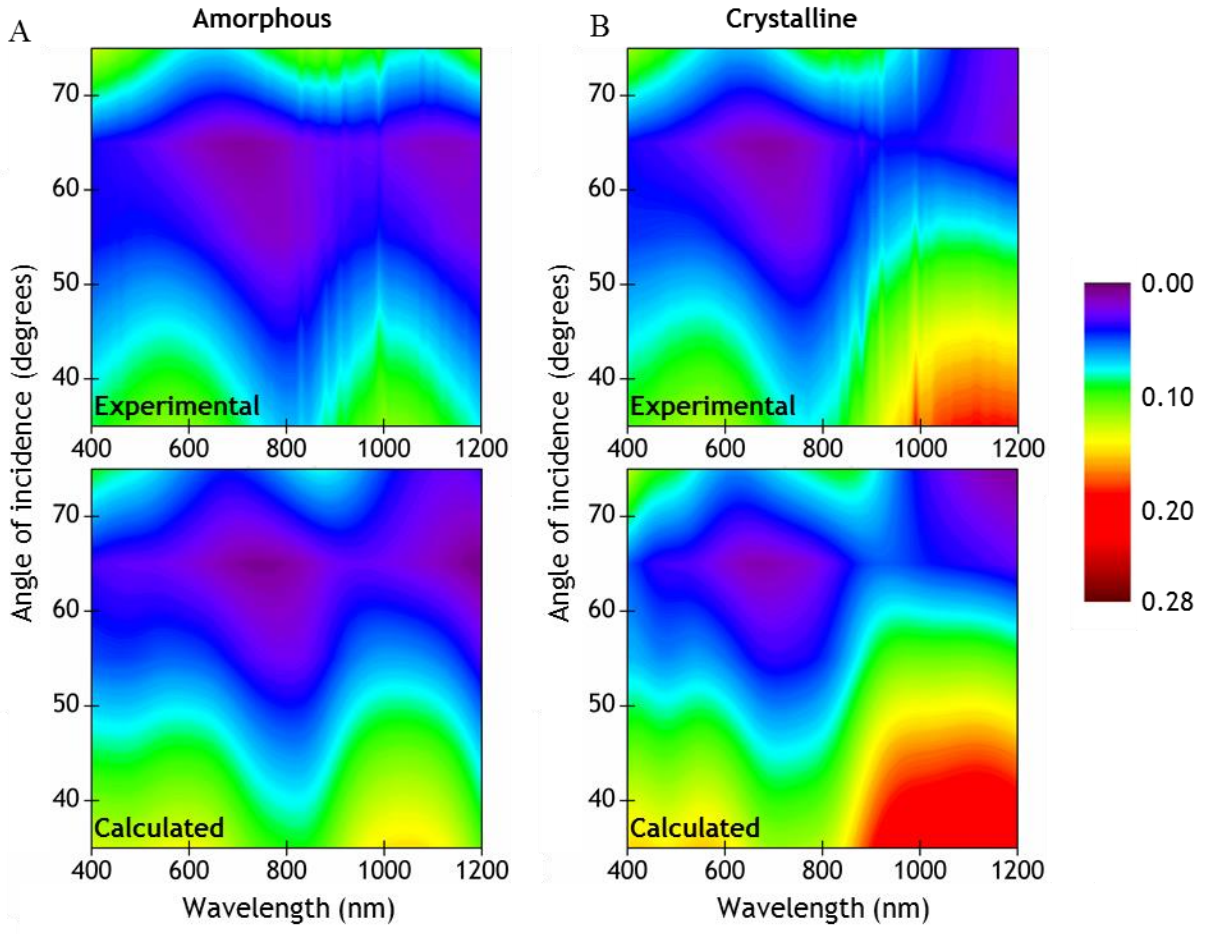

Figure 3. Experimental (top panel) and calculated (bottom panel) reflection spectra as a function of angle for TM polarized light incident on the HMM, with GST layers in the (A) amorphous, and (B) crystalline phases.

One striking feature of the reflectivity spectra in Figure 3 is that the response observed from both phases of the HMM is similar in the visible region and the difference comes up at the longer wavelengths. This has its origins in the fact that in thin GST films, the optical contrast between the two phases is significantly larger at longer wavelengths.[18]

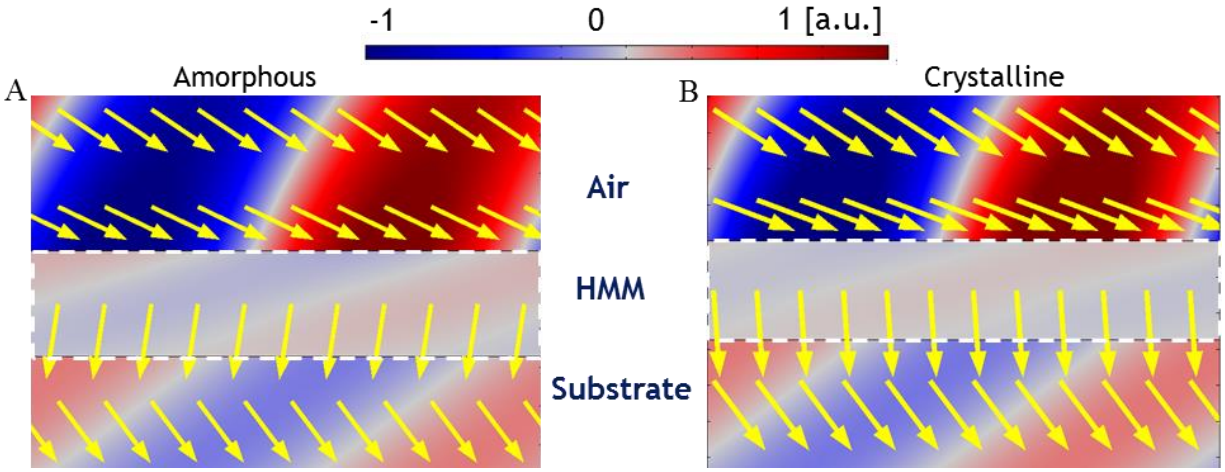

Figure 4. Colour map of the electric field amplitude and the direction of power flow for TM polarized plane wave incident at an angle of 60° on the (A) amorphous HMM and (B) crystalline HMM, at a wavelength of 1200 nm. The HMM is highlighted by white dashed lines. Spectral regime of negative refraction moves from NIR to visible by switching the phase of the GST layers from amorphous to crystalline. The simulations were performed using the experimentally determined dielectric constants of the HMM.

An intriguing aspect of materials showing type-I hyperbolic dispersion is that they also show negative refraction of the Poynting vector.[3,4] This stems from the fact that the component of the Poynting vector in the direction parallel to the layers, of the beam refracted at the interface of the HMM, is decided by the sign of $\varepsilon_{\perp}$.[1,2] We carried out finite element method (FEM) analysis of the HMM structure and simulated the electric field map and the Poynting vector for the HMM in the amorphous and crystalline phases. In the simulation, a TM polarized plane wave at 1200 nm wavelength is incident on the air-HMM interface at an angle of 60°. With the GST layers in the amorphous phase, it experiences hyperbolic dispersion with $\varepsilon_{\perp} < 0$, which in turn leads to sign

reversal of the Poynting vector component parallel to the interface resulting in negative refraction of the wave, as shown in **Figure 4A**. This is evident from the direction of the Poynting vector as well as the phase reversal of the beam refracted into the HMM. This situation is changed upon conversion of the GST layers to the crystalline phase, where the hyperbolic dispersion regime is confined to just the visible region which results in the same incident wave getting refracted positively as shown in **Figure 4B**. In the simulations, the thickness of the HMM was 273 nm , while the values of the dielectric tensor used (at λ = 1200 nm) was $\overleftrightarrow{\varepsilon}(\vec{r}) = diag(\varepsilon_{xx}, \varepsilon_{yy}, \varepsilon_{zz}) = diag(6.40 + 2.55i, 6.40 + 2.55i, -11.87 + 7.35i)$ for amorphous HMM and $diag(8.51 + 2.82i, 8.51 + 2.82i, 20.88 + 21.00i)$ for the crystalline HMM.

A full account of the dispersion shown by the HMMs in both the phases needs to consider the effects of intermixing which is understood to happen in such silver-chalcogenide thin film systems.[37–40] To achieve this, we analyzed the ellipsometry data using a layer-by-layer transfer matrix model which incorporates an intermix layer between the Ag and GST layers, whose optical constants are obtained by mixing those of the Ag and GST layers in a 50-50% ratio. We defined the thickness of the intermix layer and the imaginary part of the dielectric constant of the GST layer as the fitting parameters in the model. **Figures 5A** and **5C** show respectively, the dielectric constants of the GST and intermix layers retrieved from fitting the ellipsometry data. It is evident from these plots that the optical contrast between the two phases of GST is pronounced mainly in the NIR spectral region as is typical for a thin film of GST.[18] The thickness of the intermix layer retrieved from the model was 11.7 nm and 6.2 nm for the amorphous and crystalline HMMs, respectively. Such a reduction in the thickness of the intermix layer in chalcogenide-Ag systems upon annealing has been reported previously.[39] The validity of the transfer matrix model is confirmed by the calculated reflection spectra in **Figures 5B** and **5D** which agree reasonably well with the experimental and anisotropy model-based reflection spectra in Figure 3.

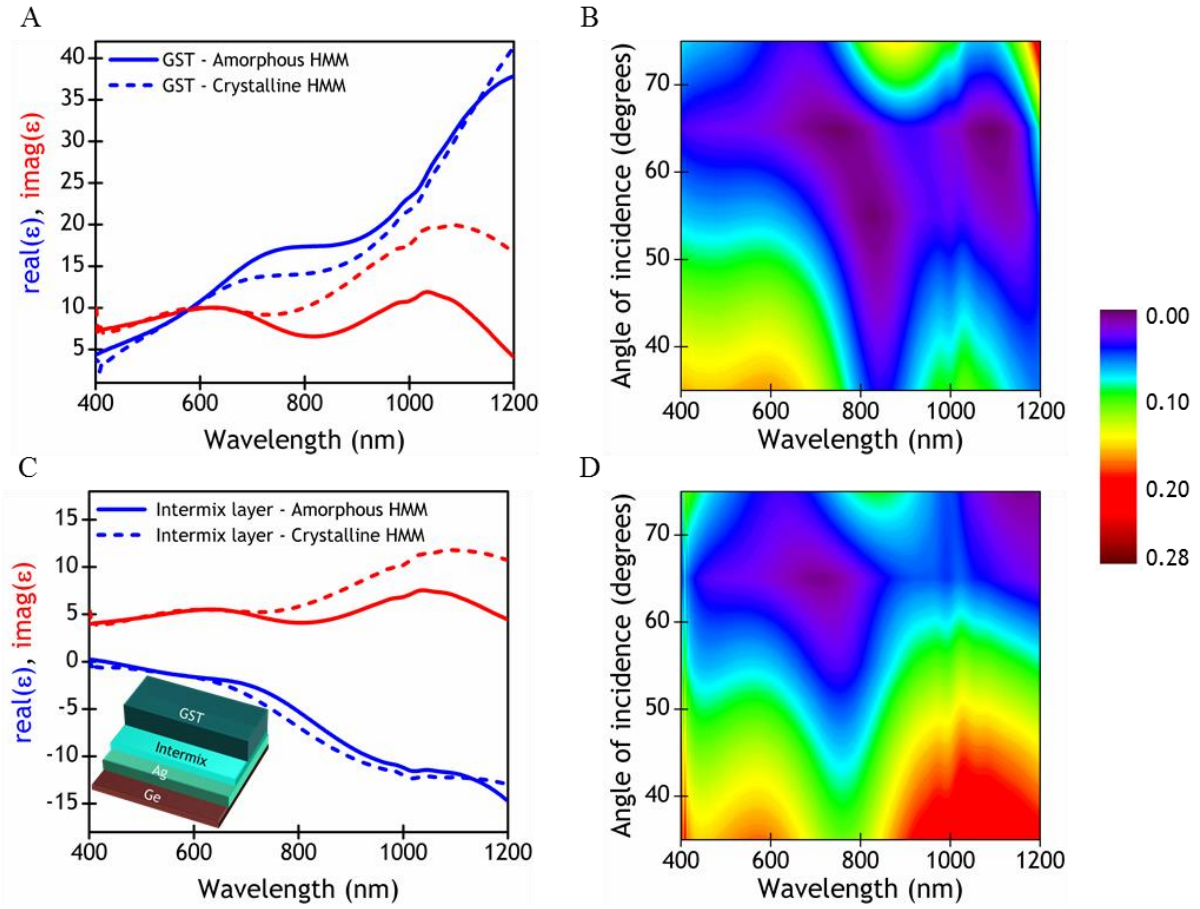

Figure 5. Real (blue) and imaginary (red) parts of the dielectric function of (A) GST and (C) intermix layers in the amorphous (solid lines) and crystalline (dashed lines) HMMs determined from the transfer matrix model. Inset of figure C shows a schematic of a single period of the layered structure with the intermix layer used in the modeling. Color maps of the angle-resolved reflection spectra for TM polarized light incident on the (B) amorphous and (D) crystalline HMMs calculated using the transfer matrix model.

The minor discrepancies between the spectra in Figures 3 and 5B may be due to additional interfacial effects beyond the simple intermixing assumed in our model. From the transfer matrix analysis, we infer that a combination of factors such as prominent optical contrast between the two GST phases in the NIR region, the existence of an intermix layer and the difference in its thickness in the amorphous and crystalline HMMs play a part in the nature of the dispersion shown in the

two phases of the HMMs; in particular, the existence of type-I hyperbolic dispersion in the NIR region in the amorphous phase and it getting confined to only the visible region upon phase change.

In conclusion, the work presented here is the first proof-of-concept demonstration of a chalcogenide-based multilayered metal-dielectric nanocomposite system and provides a platform to develop hyperbolic metamaterials capable of non-volatile switching, enabling access to hyperbolic and elliptical dispersion regions. As a proof of concept of the switchable nature of the hyperbolic response, we show that the sign of refraction in in the NIR region can be inverted by switching the phase of the chalcogenide glass. This work could pave the way towards realization of non-volatile memory hyperbolic metamaterial devices for applications in data storage, imaging, beam steering and sensing.

Supporting Information

Supporting Information is available from the Wiley Online Library or from the author. Following a period of embargo, the data from this paper can be obtained from the University of Southampton ePrints research repository, https://doi.org/xx.xxxx/SOTON/xxxx.

Acknowledgments

This research was supported by the Singapore Ministry of Education (Programmes MOE2011-T3-1-005 and MOE2016-T3-1-006) and the Engineering and Physical Sciences Research Council, UK (Project EP/M009122/1). The authors are grateful to Dr. Giorgio Adamo for useful discussions and assistance with structural characterization. Harish N. S. Krishnamoorthy and Behrad Gholipour contributed equally to this work.

Received: ((will be filled in by the editorial staff))
Revised: ((will be filled in by the editorial staff))
Published online: ((will be filled in by the editorial staff))

References

[1] A. Poddubny, I. Iorsh, P. Belov, Y. Kivshar, *Nat. Photonics* **2013**, *7*, 958.

[2] V. Podolskiy, E. Narimanov, *Phys. Rev. B* **2005**, *71*, 2.

[3] A. J. Hoffman, L. Alekseyev, S. S. Howard, K. J. Franz, D. Wasserman, V. a Podolskiy, E. E. Narimanov, D. L. Sivco, C. Gmachl, *Nat. Mater.* **2007**, *6*, 946.

[4] G. V Naik, J. Liu, A. V Kildishev, V. M. Shalaev, A. Boltasseva, *Proc. Natl. Acad. Sci. U. S. A.* **2012**, *109*, 8834.

[5] Z. Jacob, I. I. Smolyaninov, E. E. Narimanov, *Appl. Phys. Lett.* **2012**, *100*, 181105.

[6] Z. Jacob, L. V Alekseyev, E. Narimanov, *Opt. Express* **2006**, *14*, 8247.

[7] Z. Liu, H. Lee, Y. Xiong, C. Sun, X. Zhang, *Science* **2007**, *315*, 1686.

[8] M. A. Noginov, H. Li, Y. A. Barnakov, D. Dryden, G. Nataraj, G. Zhu, C. E. Bonner, M. Mayy, Z. Jacob, E. E. Narimanov, *Opt. Lett.* **2010**, *35*, 1863.

[9] Z. Jacob, J.-Y. Kim, G. V. Naik, A. Boltasseva, E. E. Narimanov, V. M. Shalaev, *Appl. Phys. B* **2010**, *100*, 215.

[10] H. N. S. Krishnamoorthy, Z. Jacob, E. Narimanov, I. Kretzschmar, V. M. Menon, *Science* **2012**, *336*, 205.

[11] Y. Guo, C. L. Cortes, S. Molesky, Z. Jacob, *Appl. Phys. Lett.* **2012**, *101*, 131106.

[12] Y. Guo, Z. Jacob, *Opt. Express* **2013**, *21*, 15014.

[13] K. Halterman, J. M. Elson, *Opt. Express* **2014**, *22*, 7337.

[14] J. Yao, X. Yang, X. Yin, G. Bartal, X. Zhang, *Proc. Natl. Acad. Sci. U. S. A.* **2011**, *108*, 11327.

[15] X. Yang, J. Yao, J. Rho, X. Yin, X. Zhang, *Nat. Photonics* **2012**, *6*, 450.

[16] K. V. Sreekanth, Y. Alapan, M. ElKabbash, E. Ilker, M. Hinczewski, U. A. Gurkan, A. De Luca, G. Strangi, *Nat. Mater.* **2016**, *15*, 621.

[17] M. J. Dicken, K. Aydin, I. M. Pryce, L. A. Sweatlock, E. M. Boyd, S. Walavalkar, J. Ma, H. A. Atwater, *Opt. Express* **2009**, *17*, 18330.

[18] B. Gholipour, J. Zhang, K. F. MacDonald, D. W. Hewak, N. I. Zheludev, *Adv. Mater.* **2013**, *25*, 3050.

[19] Q. Wang, E. T. F. Rogers, B. Gholipour, C.-M. Wang, G. Yuan, J. Teng, N. I. Zheludev, *Nat. Photonics* **2015**, *10*, 60.

[20] T. Driscoll, H.-T. Kim, B.-G. Chae, B.-J. Kim, Y.-W. Lee, N. M. Jokerst, S. Palit, D. R.

Smith, M. Di Ventra, D. N. Basov, *Science* **2009**, *325*, 1518.

[21] A. Karvounis, B. Gholipour, K. F. MacDonald, N. I. Zheludev, *Appl. Phys. Lett.* **2016**, *109*, 51103.

[22] A. Tittl, A.-K. U. Michel, M. Schäferling, X. Yin, B. Gholipour, L. Cui, M. Wuttig, T. Taubner, F. Neubrech, H. Giessen, *Adv. Mater.* **2015**, *27*, 4597.

[23] H. N. S. Krishnamoorthy, Y. Zhou, S. Ramanathan, E. Narimanov, V. M. Menon, *Appl. Phys. Lett.* **2014**, *104*, 121101.

[24] S. Dai, Q. Ma, M. K. Liu, T. Andersen, Z. Fei, M. D. Goldflam, M. Wagner, K. Watanabe, T. Taniguchi, M. Thiemens, F. Keilmann, G. C. A. M. Janssen, S.-E. Zhu, P. Jarillo-Herrero, M. M. Fogler, D. N. Basov, *Nat. Nanotechnol.* **2015**, *10*, 682.

[25] A. Kumar, T. Low, K. H. Fung, P. Avouris, N. X. Fang, *Nano Lett.* **2015**, *15*, 3172.

[26] G. Pawlik, K. Tarnowski, W. Walasik, A. C. Mitus, I. C. Khoo, *Opt. Lett.* **2014**, *39*, 1744.

[27] C. Argyropoulos, N. M. Estakhri, F. Monticone, A. Alù, *Opt. Express* **2013**, *21*, 15037.

[28] P. Li, X. Yang, T. W. W. Maß, J. Hanss, M. Lewin, A.-K. U. Michel, M. Wuttig, T. Taubner, *Nat. Mater.* **2016**, *15*, 870.

[29] C. Ríos, M. Stegmaier, P. Hosseini, D. Wang, T. Scherer, C. D. Wright, H. Bhaskaran, W. H. P. Pernice, *Nat. Photonics* **2015**, *9*, 725.

[30] B. J. Eggleton, B. Luther-Davies, K. Richardson, *Nat. Photonics* **2011**, *5*, 141.

[31] B. Gholipour, P. Bastock, C. Craig, K. Khan, D. Hewak, C. Soci, *Adv. Opt. Mater.* **2015**, *3*, 635.

[32] M. Wuttig, N. Yamada, *Nat. Mater.* **2007**, *6*, 824.

[33] D. Loke, T. H. Lee, W. J. Wang, L. P. Shi, R. Zhao, Y. C. Yeo, T. C. Chong, S. R. Elliott, *Science* **2012**, *336*, 1566.

[34] W. Chen, M. D. Thoreson, M. Campus, A. V Kildishev, V. M. Shalaev, *Opt. Express* **2010**, *18*, 5124.

[35] T. Tumkur, Y. Barnakov, S. T. Kee, M. A. Noginov, V. Liberman, *J. Appl. Phys.* **2015**, *117*, 103104.

[36] J. Orava, A. L. Greer, B. Gholipour, D. W. Hewak, C. E. Smith, *Nat. Mater.* **2012**, *11*, 279.

[37] C. C. Huang, D. W. Hewak, *Thin Solid Films* **2006**, *500*, 247.

[38] J. Orava, M. N. Kozicki, S. N. Yannopoulos, A. L. Greer, *AIP Adv.* **2015**, *5*, 77134.

[39] J. Fick, B. Nicolas, C. Rivero, K. Elshot, R. Irwin, K. A. Richardson, M. Fischer, R. Vallée, *Thin Solid Films* **2002**, *418*, 215.

[40] W. Dong, M. Krbal, J. Kalikka, X. Y. Chin, B. Gholipour, C. Soci, P. J. Fons, K. V. Mitrofanov, L. Chen, R. E. Simpson, *Thin Solid Films* **2016**, *616*, 80.

Graphical table of contents (TOC) entry

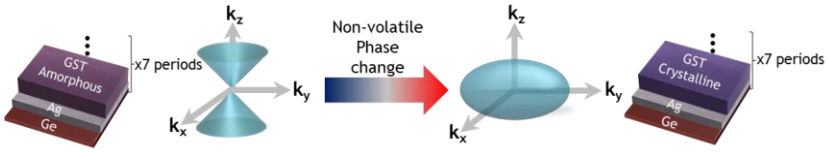

A non-volatile, reconfigurable, strongly anisotropic layered nanocomposite structure exhibiting hyperbolic dispersion is realized with $Ge_2Sb_2Te_5$ (GST) chalcogenide glass as a constituent material. By exploiting the phase change property of the GST layers in the nanocomposite, its spectral regime of hyperbolic dispersion is switched from the near-infrared to the visible.